Alonso, L., Navarro, C. & García-Castillo, S. K. (2018). Analytical models for the perforation of thick and thin thickness woven-laminates subjected to high-velocity impact. *Composites Part B: Engineering, 143*, 292–300.

DOI: 10.1016/j.compositesb.2018.01.030

**Analytical models for the perforation of thick and thin thickness woven-laminates subjected to high-velocity impact**

Luis Alonso, Carlos Navarro, Shirley K. García-Castillo*

*Department of Continuum Mechanics and Structural Analysis*

*Carlos III University of Madrid*

*Avda. de la Universidad 30, 28911-Leganés, Madrid, Spain*

**e-mail: sgcastil@ing.uc3m.es, web page: http://www.uc3m.es/mma*

**Abstract**

This paper deals with the problem of high-velocity impact of a low-mass projectile on woven composite plates. A nondimensional formulation of two analytical models has been developed (one for thin laminates and the other for thick ones). Both analytical models are based on energy conservation and have been applied for the ballistic impact on E-glass woven fibres/polyester composite plates. The results of the models (mainly the ballistic limits) have been compared with experimental results. The value of the ratio target thickness/projectile diameter determining whether the laminate behaves as thick or thin has been established.

**Keywords**

A. Laminate, B. Impact behaviour, C. Analytical modelling.

**NOMENCLATURE**

$A$ = empirical parameter

$B$ = yarn width

$b$ = stress-wave transmission factor

$C_{Vl}$ = velocity of the longitudinal elastic waves

$C_{Vt}$ = velocity of the transverse elastic waves

$C_{Vxl}$ = velocity of the compressive waves through-thickness direction

$E$ = in-plane Young modulus of the laminate plate

$E_0$ = initial kinetic energy of the projectile

$E_A$ = energy absorbed by all the energy-absorption mechanisms at any elapsed time-for thin laminate

$E_B$ = energy absorbed by all the energy-absorption mechanisms at any elapsed time for thick laminate

$E_c$ = compressive Young modulus through thickness direction of the laminate

$E_{CF1}$ = energy absorbed by compression of fibres in Region 1

$E_{CF2}$ = energy absorbed by compression of fibres in Region 2

$E_{DL}$ = energy absorbed by delamination damage

$E_{ED}$ = energy absorbed by elastic deformation of fibres

$E_{FR}$ = energy absorbed by friction between the projectile and the laminate

$E_{TF}$ = energy absorbed by tensile failure of fibres

$E_L$ = kinetic energy of the accelerated laminate during impact process

$E_{MC}$ = energy absorbed by matrix cracking

$E_{MT}$ = energy absorbed by matrix cracking per unit volume

$E_{SP}$ = energy absorbed by shear plugging

$e$ = laminate thickness

$F_{FR}$ = force recorded during the friction test

$F_{max}$ = maximum force recorded during the shear test

$G_{IICD}$ = critical dynamic-strain energy-release rate in mode II

$m_L$ = mass of the accelerated laminate formed on the back side of the plate

$m_p$ = projectile mass

$p$ = empirical parameter

$R_t$ = distance travelled by the transversal wave generated by the impact on the plate or cone radius

$R_l$ = distance travelled by the longitudinal wave on the laminate

$R_{xl}$ = distance travelled by the compressive wave along the thickness direction

$r$ = radial distance from the stagnation point in the laminate plane

$S_{sp}$ = out-plane shear failure stress of the laminate

$t$ = time elapsed during impact event

$v$ = velocity of the projectile at any instant

$v_{bl}$ = ballistic limit

$v_i$ = impact velocity of the projectile

$v_r$ = residual velocity of the projectile

$x$ = distance from the stagnation point in the thickness direction

$x_1$ = coordinate from which Stage 2 begins

$\phi_p$ = diameter of the projectile

$\varepsilon$ = in-plane strain

$\varepsilon_c$ = compressive strain along the thickness direction

$\varepsilon_r$ = in-plane failure strain of the laminate

$\varepsilon_{rc}$ = compressive failure strain of the laminate in the thickness direction

$\sigma$ = in-plane stress

$\sigma_c$ = compressive stress along the thickness direction

$\sigma_r$ = in-plane failure stress of the laminate

$\Pi_e$ = geometry ratio

$\rho_l$ = laminate density

$\rho_p$ = projectile density

$\alpha_{DL}$ = shape factor for delamination

$\alpha_{MC}$ = shape factor for matrix cracking

$\tau$ = nondimensional time

## 1.- Introduction

For their stiffness, strength, and light weight, woven laminates are commonly used in the aeronautic, maritime, and ground-transport industries as well as in civil infrastructures. These laminate structures are usually designed to withstand common loads although in some cases, they may be subjected accidentally to impact loads caused by foreign bodies. Such problems may lead to structural failure due to the low transverse stiffness that composite structures show under impact loads [1,2]. The impact velocity may vary from a few meters per second up to several hundred meters per second [3]. For instance, in the case of low-mass high-velocity projectiles striking a structure, the damage varies from indentation to perforation [4,5]. These impacts may compromise the mechanical properties of a structural element [6,7]. Therefore, engineers need predictive tools to check the structural behaviour under impact conditions. Thus, the development of analytical models, which provide sufficient accuracy for predicting the response of a composite panel under impact loads, is a hot topic.

Many previous works have examined the impact behaviour of composite laminates by means of experimental tests [4,8-13]. Although such tests are costly and time consuming, they are valid only for the configuration (plate and projectile) tested [15]. Numerical simulations have been applied successfully for

modelling the perforation process of composite structures subjected to ballistic impacts [13-18]. Such approaches require considerable computing time. However, analytical models can be useful to provide a sufficiently accurate solution with a lower computational cost than with numerical methods [9,17-27].

As a consequence of the above, there is continual interest in developing analytical models to predict the ballistic limit of laminate plates. This parameter is useful to define the condition of the perforation of a structure. The ballistic limit can be defined as the minimum velocity that a particular projectile needs to consistently penetrate the component [28].

From experimental, analytical and numerical studies, many authors have demonstrated that a fundamental parameter in the performance of a laminate plate is its thickness [4,24-26,29-36]. Some authors show a non-linear relationship between the ballistic limit and the plate thickness for E-glass plates [24,31,32]. By contrast, Zhu et al. [29] contended that there is a linear relationship between the ballistic limit and the thickness for Kevlar/polyester laminates under impact by flat-faced projectiles. Buitrago et al. [4] and Naik et al. [33] found the same behaviour for E-Glass woven laminates subjected to high-velocity impact with spherical and flat-faced projectiles, respectively. Additionally, these studies show that there is a certain controversy regarding how to consider a laminate as being thick or as thin. For example, the work by Caprino et al. [34] shows that laminates of less than 6 mm may be considered as thin for graphite/epoxy laminates, in agreement with García-Castillo et al. [17,36] but for E-Glass laminates. On the other hand, there are works where laminates are considered thick when exceeding 2 mm [32] for E-Glass/polyester or 4 mm [30] for graphite/epoxy laminates. The works by Naik et al. [33,35] have demonstrated that the thickness of a laminate determines the energy-absorption mechanisms to consider for the analytical models. Therefore, definition of laminates as thin or thick is a key issue in high-velocity impacts.

In the present study, the objective is to estimate the threshold thickness that determines the behaviour of a laminate plate as thin or thick. This threshold is important because it establishes the energy-absorption mechanisms to consider. To reach this goal, a nondimensional formulation of the two models was developed.

**2.- Model description**

Two analytical models for woven laminates (thin and thick) of glass fibres in polymer resin used in previous works [17,35] were modified in this study. Both models considered that the kinetic energy of the projectile impact is consumed during the perforation process by several energy-absorption mechanisms.

In the case of thin laminates, the energy-absorption mechanisms are: tensile failure of fibres, elastic deformation of fibres, acceleration of the laminate in the back-side of the plate, delamination and matrix cracking. On the other hand, the energy-absorption mechanisms considered for thick laminates are: compression, tensile failure of fibres, delamination, matrix cracking, shear plugging and friction.

In this work, both models have been expressed in a nondimensional form using the Vaschy-Buckingham Π Theorem in order to reduce the number of parameters on which the problem depends.

The models studied depend on three elemental magnitudes: mass[M], length[L], and time[T], which may be written in their nondimensional form as follows:

$$[\mathrm{M}] = \rho_p \, \phi_p^3 \qquad (1) \qquad [\mathrm{L}] = \phi_p \qquad (2) \qquad [\mathrm{T}] = \frac{\phi_p}{V_i} \qquad (3)$$

The nondimensional time *(τ)* is defined as the integration variable.

***2.1.- Analytical model for thin woven laminates***

The analytical model for thin woven laminates shown in this work is based on a previous model developed by García-Castillo et al. [17]. Nevertheless, this model has been improved to consider the spherical geometry of the projectile. Since this approach is based on energy criteria, the previously mentioned energy-absorption mechanisms are considered. This can be expressed as in the following equation. A detailed description of the expressions for each mechanism can be found in García-Castillo et al. [17].

$$\overline{E_A} = \overline{E_L} + \overline{E_{TF}} + \overline{E_{ED}} + \overline{E_{DL}} + \overline{E_{MC}} \qquad (4)$$

The following hypotheses have been assumed in the model formulation:

- The projectile is rigid and thus it remains undeformable over the entire impact process.
- The laminate performance is considered linear-elastic and transversely isotropic.
- The transversal and longitudinal wave velocities in the laminate remain constant over the entire process.
- The energies absorbed by tensile failure and elastic deformation of fibres are treated independently.
- The back-side of the laminate is subjected to acceleration by the projectile.
- The energies absorbed by friction and shear plugging are considered negligible.
- The energy absorbed by heat transfer between the projectile and the laminate is disregarded.

The problem depends on 14 fundamental parameters which are: $e$, $\rho_l$, $E$, $\varepsilon_r$, $\sigma_r$, $\phi_p$, $\rho_p$, $V_i$, $E_{MT}$, $G_{IICD}$, $\alpha_{DL}$, $\alpha_{MC}$, $B$, and $b$.

When the equations of the models are expressed in a nondimensional way, several Π groups appear. The

problem depends on the following Π groups: $\Pi_e = \frac{e}{\phi_p}$, $\Pi_{\rho_l} = \frac{\rho_l}{\rho_p}$, $\Pi_{\sigma_r} = \frac{\sigma_r}{\rho_p V_l^2}$, $\Pi_E = \frac{E}{\rho_p V_l^2}$, $\Pi_{G_{IICD}} = \frac{G_{IICD}}{\rho_p V_l^2 \phi_p}$, $\Pi_{E_{MT}} = \frac{E_{MT}}{\rho_p V_l^2}$, $\Pi_B = \frac{B}{\phi_p}$, $\alpha_{DL}$, $\alpha_{MC}$, $b$, $\varepsilon_r$. According to the Vaschy-Buckingham Π Theorem, the number of parameters on which the problem depends has been reduced from 14 to 11.One of the key Π groups of the problem is the geometry ratio ($\Pi_e$), which will be analysed in further detail in the Results section.

In the present work, the symbol $\bar{}$ over any of the variables of the problem means nondimensionality

*2.1.1.- Energy absorbed by laminate acceleration*

For the calculation of the kinetic energy absorbed by laminate acceleration throughout the impact process, it was assumed that this part of the laminate moves at just the same velocity as the projectile. This zone of the laminate is affected by the transverse elastic wave and thus, it grows with time. In a generic time, the normalized velocity of this wave is:

$$C_{V_t} = \sqrt{(1+\varepsilon_r)\frac{\Pi_{\sigma_r}}{\Pi_{\rho_l}}} - \sqrt{\frac{\Pi_E}{\Pi_{\rho_l}}}\varepsilon_r \tag{5}$$

It has to be noticed that $C_{V_t}$ is not a Π group of the problem but a combination of Π groups. Therefore, the radius of the moving zone of the laminate is:

$$\overline{R_t}(\tau) = C_{V_t}\tau \tag{6}$$

The mass of the zone of the laminate accelerated at the projectile velocity can be determined as:

$$\overline{m_L}(\tau) = \pi \Pi_e \Pi_{\rho_l} \overline{R_t}(\tau)^2 \tag{7}$$

Consequently, the kinetic energy absorbed by this zone of the laminate is:

$$\overline{E_L}(\tau) = \frac{1}{2}\overline{m_L}(\tau)\bar{v}(\tau)^2 \tag{8}$$

*2.1.2.- Energy absorbed by tensile failure of fibres*

The fibres that are directly impacted just below the projectile undergo tensile failure. Their strain depends on the radial distance to the projectile due to the wave attenuation.

$$\varepsilon(\bar{r}) = \varepsilon_r b^{\frac{\bar{r}}{\Pi_B}} \tag{9}$$

The longitudinal velocity determines the fibre length affected by that strain:

$$C_{V_l} = \sqrt{\frac{\Pi_E}{\Pi_{\rho_l}}} \tag{10}$$

Therefore, the distance travelled by the longitudinal wave is:

$$\bar{R}_l(\tau) = C_{V_l}\tau \tag{11}$$

For symmetry reasons the total fibre length subjected to strain is $2\bar{R}_l(\tau)$.

Consequently, the energy absorbed by tensile failure of fibres can be expressed as:

$$\overline{E_{TF}}(\tau) = \int_0^{\tau} \frac{1}{2}\left[\Pi_E \Pi_B \bar{v}(\tau) \int_0^{2\overline{R_l}(\tau)} \varepsilon_r b \frac{\bar{r}}{\overline{\Pi_B}} d\bar{r}\right] d\tau \tag{12}$$

*2.1.3.- Energy absorbed by elastic deformation of fibres*

The fibres deformed elastically during impact lie within the region affected by the transversal stress wave generated by the impact. This region is located between the projectile diameter and the distance covered by the transversal wave. Since the projected area in contact with the laminate changes with the position, an effective diameter has been defined:

$$\bar{\phi}(\bar{x}) = \begin{cases} 2\sqrt{\bar{x} - \bar{x}^2} & if\ \bar{x} < 0.5 \\ 1 & if\ \ \bar{x} \geq 0.5 \end{cases} \tag{13}$$

The profile of strains along a fibre between the projectile perimeter and the transverse wave radius is assumed to be linear as in the model of García-Castillo et al. [17]. Therefore, the energy absorbed by elastic deformation of fibres is given by:

$$\overline{E_{ED}}(\tau) = \pi \Pi_E \Pi_e \varepsilon_r^2 \int_{\frac{\bar{\phi}(\bar{x})}{2}}^{\overline{R_t}(\tau)} \left[\frac{2(\overline{R_t}(\tau) - \bar{r})}{2\overline{R_t}(\tau) - \bar{\phi}(\bar{x})}\right]^2 \bar{r} d\bar{r} \tag{14}$$

*2.1.4.- Energy absorbed by delamination and matrix cracking*

The energy absorbed due to damage by delamination and matrix cracking is a result of the acceleration on the back side of the laminate. Therefore, it is a result of the distance covered by transversal waves on the laminate. It was assumed that the area that contributes to the absorption mechanism by delamination and matrix cracking is approximately equal to a circular surface.

Consequently, the energy absorbed by delamination can be calculated as:

$$\overline{E_{DL}}(\tau) = \pi \Pi_{G_{IICD}} \overline{R_t}(\tau)^2 \alpha_{DL} \tag{15}$$

The energy absorbed by matrix cracking can be calculated as:

$$\overline{E_{MC}}(\tau) = \pi \Pi_{E_{MT}} \Pi_e \overline{R_t}(\tau)^2 \alpha_{MC} \tag{16}$$

*2.1.4.- Model formulation*

The proposed model has been established by means of an energy balance. That is:

$$1 = \bar{v}(\tau)^2 + \frac{12}{\pi} \overline{E_A}(\tau) \tag{17}$$

Two functions are defined in order to facilitate the handling of the equations:

$$\bar{h}(\tau) = \Pi_B \int_0^{2\overline{R_l}(\tau)} \left( \int_0^{\varepsilon(\bar{r})} \bar{\sigma}(\varepsilon) d\varepsilon \right) d\bar{r} \tag{18}$$

and

$$\bar{g}(\tau, \bar{x}, \bar{v}) = -\frac{d}{d\tau} \left[ \pi \Pi_E \Pi_e \varepsilon_r^2 \int_{\frac{\bar{\phi}(\bar{x})}{2}}^{\overline{R_t}(\tau)} \left[ \frac{2(\overline{R_t}(\tau) - \bar{r})}{2\overline{R_t}(\tau) - \bar{\phi}(\bar{x})} \right]^2 \bar{r} d\bar{r} + \overline{R_t}(\tau)^2 \left( \pi \Pi_{G_{IICD}} \alpha_{DL} + \pi \Pi_{E_{MT}} \Pi_e \alpha_{MC} \right) \right] \tag{19}$$

Derivation of the above-mentioned energy balance with respect to time, reorganization of the equation, and introduction of these functions give the following non-linear second-order differential equation. It can be solved by numerical methods, once the initial conditions have been stated:

$$\frac{d^2\bar{x}(\tau)}{d\tau^2} = \frac{\bar{g}(\tau, \bar{x}, \bar{v}) - \frac{d\bar{x}(\tau)}{d\tau} \bar{h}(\tau) - \pi \Pi_e \Pi_{\rho_l} C_{V_t}{}^2 \tau \left( \frac{d\bar{x}(\tau)}{d\tau} \right)^2}{\pi \frac{d\bar{x}(\tau)}{d\tau} \left( \frac{1}{6} + \Pi_e \Pi_{\rho_l} C_{V_t}{}^2 \tau^2 \right)} \tag{20}$$

$$\bar{x}(0) = 0$$

$$\bar{v}(0) = 1$$

***2.2.- Analytical model for thick woven laminates***

Thick woven laminates do not behave in the same way as thin laminates, as demonstrated by Naik et al. [35] and García-Castillo et al. [17,36]. This model is based on energy criteria and the energy-absorption mechanisms considered are the previously mentioned. These energy-absorption mechanisms considered are the same as those used by Naik et al. [30], but the hypotheses, the stages in which the impact event is divided, and also the formulation, are quite different.

$$\overline{E_B} = \overline{E_{CF1}} + \overline{E_{CF2}} + \overline{E_{TF}} + \overline{E_{DL}} + \overline{E_{MC}} + \overline{E_{SP}} \tag{21}$$

The following hypotheses in model formulation have been considered:

- The projectile is rigid and thus it remains undeformable over the entire impact process.
- The laminate performance is considered linear-elastic and transversely isotropic.
- The wave velocities in the laminate remain constant over the entire process.
- The energy absorbed by compression is related to the compressive wave velocity throughout the thickness direction.
- The energy absorbed by compression is divided in two regions (Fig. 1), the fibres that are located directly under the projectile (Region 1) and the rest of the fibres affected by the compressive waves (Region 2).

- The energy absorbed by shear plugging takes place in the projectile perimeter in the thickness direction.
- The impact event is divided in two steps: in the first one the following energy-absorption mechanisms act: compression, tensile failure of fibres, delamination, matrix cracking and shear plugging. In the second stage only the friction takes place.
- The Stage 1 ends with the complete failure of the laminate.
- The failure criteria considered which determines the transition from Stage 1 to Stage 2 is the complete laminate failure by compression.
- The energy absorbed by heat transfer between the projectile and the laminate is considered negligible.

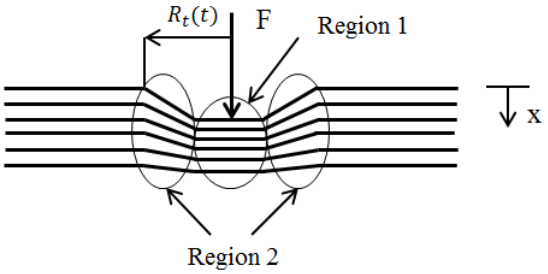


*Fig. 1. Regions considered for the compression*

The problem in the first stage depends on 17 fundamental parameters which are: $e$, $\rho_l$, $E$, $\varepsilon_r$, $\sigma_r$, $\phi_p$, $\rho_p$, $V_i$, $E_{MT}$, $G_{IICD}$, $\alpha_{DL}$, $\alpha_{MC}$, $B$, $b$, $\varepsilon_{rc}$, $E_c$ and $S_{sp}$. In addition to the Π groups that appears in the problem for thin laminates, three new Π groups appear for the formulation for thick woven laminates: $\Pi_{E_c} = \frac{E_c}{\rho_p V_i^2}$, $\Pi_{S_{sp}} = \frac{S_{sp}}{\rho_p V_i^2}$, $\varepsilon_{rc}$. According to the Vaschy-Buckingham Π Theorem, the number of parameters on which the problem depends has been reduced from 17 to 14.

As before, at the moment of the impact, several waves propagate in different directions. These travel at velocities which depend on the material properties and the direction because of the material anisotropy. The model developed here considers three different wave velocities: the longitudinal wave (Eq. 10), transverse wave (Eq. 5) and, compressive wave over the thickness direction:

$$\mathrm{C}_{V_{xl}} = \sqrt{\frac{\Pi_{E_c}}{\Pi_{\rho_l}}} \tag{22}$$

Consequently, the distance travelled by this compressive wave at any time is given by:

$$\overline{R_{xl}}(\tau) = \mathrm{C}_{V_{xl}}\tau \tag{23}$$

In this new model, two stages were considered, in contrast with Naik et al. [30], who considered three stages. The following explains why the event can be divided in two stages instead of three.

*Stage 1*

When the projectile impacts on the plate, several waves propagate in different directions. The compressive wave in the thickness direction has been considered, in contrast to the model for thin laminates.

It was assumed that the first stage (Fig. 2) begins when the projectile impacts on the plate and it ends when the laminate fails completely. The model of Naik et al. [35] has an intermediate stage between the moment the compressive wave in the thickness direction reaches the back face of the plate and the complete failure of the laminate. However, this stage is very short in time and the amount of energy absorbed by compression is small, as Naik et al. demonstrated [35]. For this reason, in the model developed the intermediate stage was not considered and Stage 1 continues until the laminate completely fails by compression.

*Stage 2*

In the present work, it was assumed that the laminate fails and Stage 2 begins (Fig. 2) when all the yarns reach the maximum compressive strain. In Stage 2 a plug is formed and the only energy-absorption mechanism that is taken into account is the friction between the projectile and the laminate and the possible resistance of the plug through the laminate.

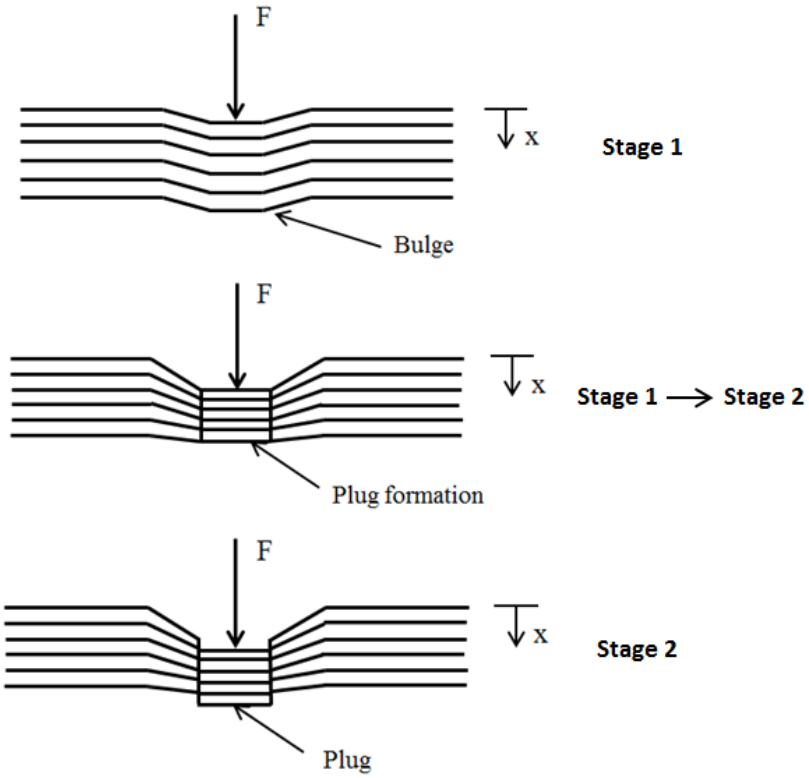


*Fig. 2. Plug formation during the impact*

*2.2.1.- Energy absorbed by compression*

The energy absorbed by compression can be divided into two different regions (Fig. 1). Region 1 is formed by the fibres just below the projectile and Region 2 is the one from the projectile perimeter to the distance travelled by the transverse wave (Eq. 6).

The energy absorbed by compression in Region 1 is:

$$\overline{E_{CF1}}(\tau) = \frac{\pi}{4}\left[\int_0^{\varepsilon_{rc}} \bar{\sigma_c}(\varepsilon_c) d\varepsilon_c\right] \overline{R_{xl}}(\tau) \tag{24}$$

The elastic compressive strain is assumed linear in Region 2. The energy absorbed by this mechanism is:

$$\overline{E_{CF2}}(\tau) = \pi \Pi_{E_c} \Pi_e \varepsilon_{rc}^2 \int_{0.5}^{\overline{R_t}(\tau)} \left[\frac{2(\overline{R_t}(\tau) - \bar{r})}{2\overline{R_t}(\tau) - 1}\right]^2 \bar{r} d\bar{r} \tag{25}$$

*2.2.2.- Energy absorbed by tensile failure of fibres*

Tensile failure of fibres occurs at the yarns of Region 2 (Fig. 1). These yarns are also subjected to a tensile stress in the radial direction. It is assumed that the strain is maximum in the projectile perimeter and minimum in the radius of the longitudinal wave. Therefore, the energy absorbed by tensile failure of fibres is the one expressed in the Equation 12.

*2.2.3.- Energy absorbed by delamination and matrix cracking*

The energy absorbed by delamination and matrix cracking are the same as those found for thin laminates (Eqs.15 and16).

*2.2.4.- Energy absorbed by the formation of shear plugging*

When a thick woven laminate is subjected to high-velocity impact, the shear stress through the thickness near the projectile periphery rises. If this stress exceeds the shear-plugging strength ($S_{sp}$), then the failure occurs and a shear plug is formed. Consequently, the energy absorbed by shear plugging is:

$$\overline{E_{SP}}(\tau) = \pi \int_0^{\tau} \bar{v}(\tau) \Pi_{S_{sp}} \Pi_e d\tau \tag{26}$$

*2.2.5.- Energy absorbed by friction*

Once the material has failed, Stage 2 starts and friction is the only energy-absorption mechanism acting. It can be observed that the energy absorbed by friction depends on position instead of time:

$$\overline{E_{FR}}(\bar{x}) = \overline{F_{FR}}\left(\bar{x} - \frac{x_1}{\phi_p}\right) \tag{27}$$

*2.2.6.- Model formulation*

For Stage 1, the model has been formulated through an energy balance:

$$1 = \bar{v}(\tau)^2 + \frac{12}{\pi}\overline{E_B}(\tau) \tag{28}$$

Two functions have been defined in order to facilitate the handling of the equations:

$$\bar{h}(\tau) = \Pi_B \int_0^{2\overline{R_l}} \left( \int_0^{\varepsilon(\bar{r})} \bar{\sigma}(\varepsilon) d\varepsilon \right) d\bar{r} + \pi \Pi_{S_{sp}} \Pi_e \tag{29}$$

$$\bar{g}(\tau) = -\frac{d}{d\tau}\left[ \pi \Pi_{E_c} \Pi_e \varepsilon_{rc}^2 \int_{0.5}^{\overline{R_t}} \left[ \frac{2(\overline{R_t}(\tau) - \bar{r})}{2\overline{R_t}(\tau) - 1} \right]^2 \bar{r} d\bar{r} + \overline{R_t}(\tau)^2 \left( \pi \Pi_{G_{IICD}} \alpha_{DL} + \pi \Pi_{E_{MT}} \Pi_e \alpha_{MC} \right) \right] \tag{30}$$

As before, by deriving this balance with respect to time (Eq. 28), reorganizing the equation, and introducing these functions, the following non-linear second-order equation, which can be solved by numerical methods with the corresponding initial conditions, is formulated:

$$\frac{d^2\bar{x}(\tau)}{d\tau^2} = \frac{\bar{g}(\tau) - \frac{d\bar{x}(\tau)}{d\tau}\bar{h}(\tau) - \frac{\pi}{8} C_{V_{xl}} \Pi_{E_c} \varepsilon_{rc}^2}{\frac{\pi}{6}\frac{d\bar{x}(\tau)}{d\tau}} \tag{31}$$

$$\bar{x}(0) = 0$$

$$\bar{v}(0) = 1$$

It has to be stated that the Eq. 31 is valid only for Stage 1. Therefore, when the Stage 1 ends and Stage 2 starts, only the friction and the possible resistance of the plug take place. Since this moment, the Eq. 27 is employed.

**3.- Materials and experimental procedures**

In this study, E-glass/polyester woven laminates were considered. These laminates are widely used in naval and ground-transport industries because of their good mechanical properties, low manufacturing costs and permeability to electromagnetic waves. Although these kinds of structures are not designed as armour, they could be subjected to high-velocity impacts of low-mass fragments, and this requires fuller knowledge of their response to impacts of this type. In this work, impact tests were carried out on laminates of 9 mm thick. Besides, friction and shear tests were performed on laminates of 9 mm and 12 mm thick. The purposes of the impact tests were to validate the analytical models. On the other hand, the friction and shear tests were made to estimate the properties and variables required by the analytical models.

Also, a set of tests were applied to determine different mechanical properties for the material. The first was a friction test to determine the friction force acting between the projectile and the laminate once the perforation process begins and the projectile is breaking through the laminate. In a second phase, the transverse (out of plane) plugging shear resistance of the laminate was measured with the same

experimental device. The friction and shear tests were conducted on a servohydraulic test machine (Instron 8516) with loading rates of 1 mm/min applied to specimens. Additionally, a set of impact tests were made using a gas gun to shoot a steel ball 7.5 mm in diameter against a laminate.

### *3.1.- Friction test*

A specific experimental device based on that developed by Pandya et al. [37] was designed with modifications to adapt the tool to the available servohydraulic test machine of the laboratory and according to ASTM Standard D 732-02 [38]. The modifications were: the geometry was cylindrical with four highlights to centre the laminate, as depicted in Fig. 3. The two tapes (upper and lower) connected by the screws prevent the laminate from bending during the test. The punch for the friction test has a cleft so that it can adapt to the projectile. The specimens of the material used in the test measured 50 mm x 50 mm, all with a cylindrical through-thickness hole at their centres. The hole diameter in the laminate (7.4 mm) was slightly smaller than the projectile ball (7.5 mm). When the punch moved down it pushed the projectile through the laminate and the friction force vs. the displacement was recorded.

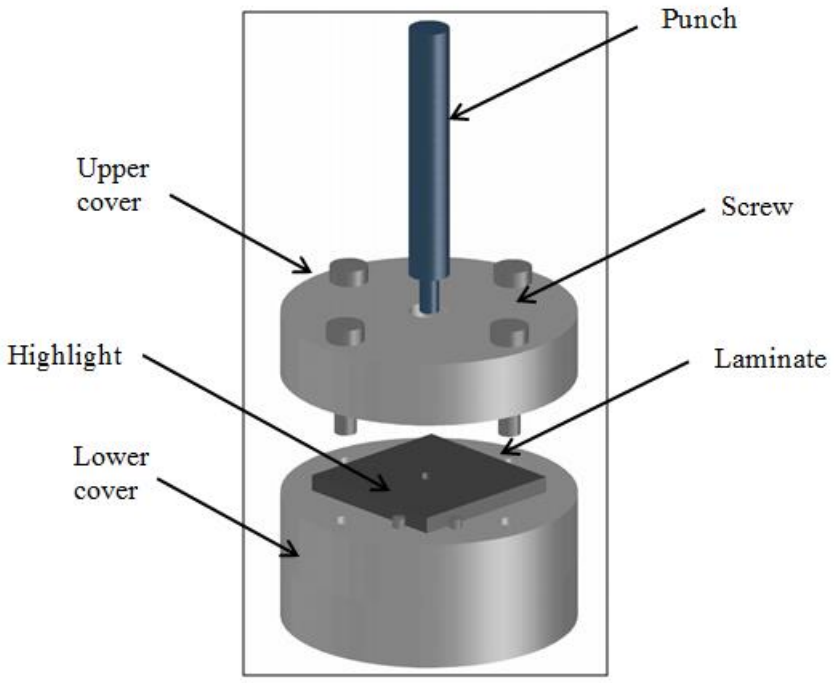


*Fig. 3. Specific tool for friction and shear tests*

### *3.2.- Shear test*

The objective of these tests was to determine the material properties throughout the thickness direction needed for the thick-laminate model. The experimental device was the same as used in the friction tests, the difference being in the punch used for this experimental case that is, the punch did not have a cleft and

its diameter was smaller.

In these tests, specimens of the same dimensions as before were used but the through thickness diameter was 6 mm. The first part of this punch was inserted into the laminate and guided the movement. When the punch moved down it pushed a part of the laminate through the thickness direction and the force vs. the displacement was recorded. From this data, the ultimate shear strength was calculated from the following equation:

$$S_{SP} = \frac{F_{max}}{\pi \phi_p e} \tag{32}$$

The properties required for the models were taken from previous work of one of the authors [14] and the others are shown in the Table 1.

| Symbol | Property | Unit | Value |
|---|---|---|---|
| $E_{c3}$ | Compressive Young Modulus out of plane | $[MPa]$ | 1052.1 |
| $\varepsilon_{rc3}$ | Ultimate compressive strain out of plane | | 0.1607 |
| $S_{SP}$ | Shear resistance out of plane | $[MPa]$ | 134.3 |

*Table 1. Properties in the thickness direction*

### *3.3.- Impact test*

The laminate plates of E-glass/polyester plain weave and 9 mm in thickness were impacted in this test. The dimensions of the specimens tested were 150 mm x 150 mm. This specimen size ensured that the damage did not reach the edge of the specimen. Therefore, the boundary conditions did not influence the damage area [17]. The conditions of the tests were the same as those taken into consideration by Buitrago et al. [4]

The experimental impact tests were made using an A1G+gas gun (manufactured by Sabre Ballistics). The specimens were impacted by spherical steel projectiles of 1.725 g in mass and 7.5 mm in diameter.

The impact tests were recorded by a high-speed video camera (APX PHOTRON FASTCAM) with a data-acquisition system capable of taking up to 120,000 frames per second. For better recording quality, a high-intensity light source, model ARRISUN 12 plus, was used. From the information provided by the camera, the impact and residual velocities were calculated, evaluating the distance travelled by the projectile in several consecutive frames.

As is known, the ballistic limit cannot be established in a determinist way because for certain values it cannot be known whether complete perforation occurs. In addition, the residual velocity of the projectile from the gas gun cannot be totally controlled with sufficient precision. Therefore, in this study, the ballistic limit has been estimated using the Lambert and Jonas [3] equation (Equation 33), which is given below, by a least-square-fitting method.

$$v_r = A(v_i^p - v_{bl}^p)^{1/p} \quad (33)$$

The ballistic limit for the considered projectile and for a target made on E-glass/polyester composite 9 mm thick is 428.4 ± 1.7 m/s.

**4.- Model verification**

For the validation of the analytical models, the ballistics of the laminates made of E-glass/polyester woven plies of various thicknesses (3 mm, 6 mm, 9 mm, and 12 mm) were analytically determined and then compared with those experimentally measured. For the case of the impact on the laminate plate 9 mm thick, experiments were carried out in this work and, for the cases of 3 mm, 6 mm, and 12 mm the results were taken from previous experiments for the same projectile and conditions as found in reference [4]. The laminate properties were taken from the previous work [17].

Table 2 shows the ballistic limits found in the experiments together with those predicted by the two analytical models developed (one for thin and the another for thick laminates). The analytical model for thick laminates accurately predicts the ballistic limit for 9-mm and 12-mm laminates but the thick-laminate model does not properly predict the ballistic limit for laminate thicknesses of less than 6 mm. However, there was excellent agreement (error <10%) between the analytical predictions and the experimental results when using the thin-laminate model for laminates 3 mm and 6 mm thick. It bears noting that the model for thick laminates fits the experimental results (9 mm and 12 mm) with an error below 1.5%.

| **Plates** | **Ballistic limit (m/s)** | | | | |
|---|---|---|---|---|---|
| | | Analytical Model | | Error (%) | |
| | Experimental | Thick laminates | Thin laminates | Thick laminates | Thin laminates |
| **3 mm[3]** | 212 | 329.5 | 192.5 | 55.42 | 9.20 |
| **6 mm[3]** | 332 | 385.5 | 339.5 | 16.61 | 2.26 |
| **9 mm[** | 428 | 433.5 | 494.5 | 1.29 | 15.54 |
| **12 mm[3]** | 550 | 543.5 | 617.5 | 1.18 | 12.27 |

*Table 2. Experimental and analytical results of the ballistic limit*

Moreover, it has been confirmed that the ballistic limit is independent of the projectile geometry for thin laminates. For projectiles having the same mass and diameter, this was confirmed in previous works of Gellert et al. [31] and Garcia-Castillo et al. [36]. Therefore, the analytical models enable an accurate estimation of the ballistic limit for thin GFRP woven laminates. Also, the formulation of the model enables a calculation of the absorbed energy for each energy-absorption mechanism, and hence the total energy absorbed by the laminate.

**5.- Results**

The ratio of laminate thickness/projectile diameter (herein called the geometry ratio) is a parameter to consider in the high-velocity-impact studies, as demonstrated by other studies [39]. Therefore, in this work the results of this ratio are discussed.

Fig. 4 shows the variation of the ballistic limit regarding the geometry ratio from both analytical models mentioned above. As reflected in this figure the intersection between the two curves occurs for a geometry ratio equal to 0.94. Therefore, the threshold thickness for the laminates studied is around 7.05 mm. The estimation errors between the results for those analytical models and the experimental results can be seen in Fig. 5. The two curves intersect for a geometry ratio equal to 0.98, which is associated with a thickness equal to 7.35.mm. Therefore, it could be assessed that the threshold thickness (thickness at which the laminate behaves as a thick one) for the woven laminates of E-glass/polyester studied experimentally is between 7 mm and 7.5 mm. This thickness interval is near the projectile diameter, where the geometry ratio is around 1. This result agrees with that reported by Rosenberg et al. [40] for metal plates subjected to high-velocity impact. These authors observed that the relevant parameter in impact modelling is the geometry ratio. It may be concluded that, as in metal targets, composite plates can be classified as:

- Thin plates: $e/\Phi_p << 1.0$
- Thick plates: $e/\Phi_p >> 1.0$

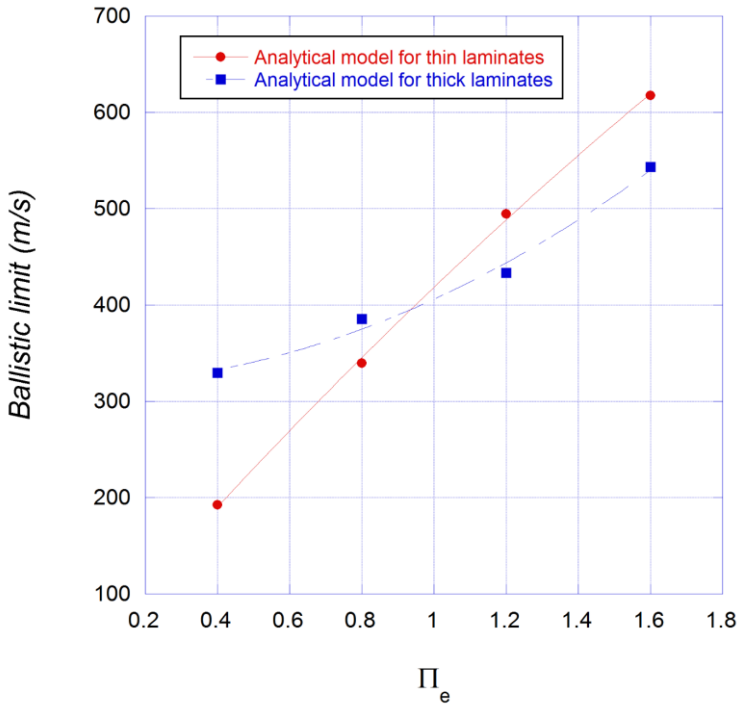

*Fig. 4. Variation of the ballistic limit vs. the geometry ratio estimated from both analytical models*

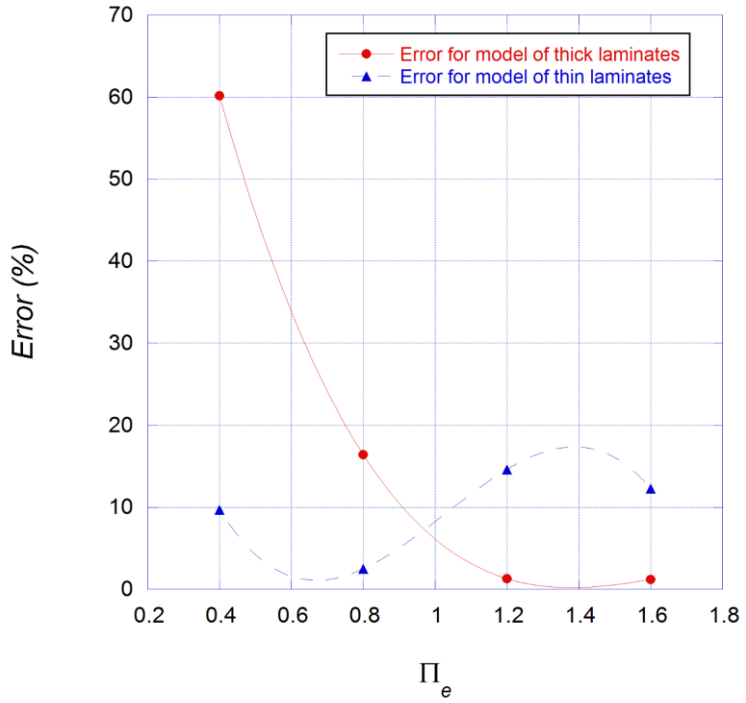


*Fig. 5. Error of the analytical models in the prediction of the ballistic limit*

For the confirmation of these observations a set of new impact analytical simulations were conducted to estimate the threshold thickness that determines the performance of the laminates as thin or thick. Table 3 shows a summary of the studies carried out with the analytical models for other projectile diameters and thus, different geometry ratios. Once again, the results showed that the transition between the applicability of thin and thick analytical models takes place when the geometry ratio is around 1.

| **Diameter (mm)** | $\Pi_e$ |
|---|---|
| **5** | 1.11 |
| **6.5** | 0.98 |
| **7.5** | 0.94 |
| **8.5** | 0.86 |
| **10** | 0.84 |
| **Average** | 0.946 |
| **Typical deviation** | 0.108 |

*Table 3. Geometry ratio at the threshold for different diameters*

Table 4 shows the differences in the prediction of the two models (thin and thick) for a value of a geometry ratio equal to 1 with different projectile diameters. It can be pointed out that the differences are less than 7% for all the cases.

| **Diameter (mm)** | $v_{bl}$ **(m/s)** | | **Difference (%)** |
|---|---|---|---|
| | **Thin** | **Thick** | |
| **5** | 283.7 | 303.1 | 6.84 |
| **6.5** | 365.1 | 361.4 | 1.01 |

| | | | |
|---|---|---|---|
| **7.5** | 418.5 | 406.1 | 2.96 |
| **8.5** | 472.6 | 444.8 | 5.88 |
| **10** | 555.3 | 526.4 | 5.20 |

*Table 4. Prediction of the ballistic limit for* $\Pi_e = 1$

To study the energy-absorption mechanisms four geometry ratios were considered. Two geometry ratios less than 1 (0.4 and 0.8) and, other two more than 1 (1.2 and 1.4) were chosen and, for each analytical simulation, only the impact at the ballistic limit was considered. Figs. 6 and 7 show the time course of the energy absorbed by the different mechanisms during the perforation of laminates for geometry ratios of less than 1 (Fig. 6) and for those of more than 1 (Fig. 7). The normalized energy appears in a natural way in the nondimensional formulation of the problem and it corresponds with the ratio of the energy absorbed by different mechanisms normalized to the projectile kinetic energy.

Fig. 6 shows that the most important energy-absorption mechanism is elastic deformation of fibres, which represents more than 50%. An increase in the geometry ratio (Fig. 6b) leads to greater absorbed energy by the fibres during elastic deformation. The energy absorbed by tensile failure of fibres is the second energy-absorption mechanism in importance but, decreases with the geometry ratio, as observed by García Castillo et al. .[36]. Another important result is that the energy of the moving cone rose to a certain value and then fell when the laminate returned to its original position. Finally, the contribution to energy absorption of matrix cracking and delamination mechanisms proved minor.

When the geometry ratio increases (Fig. 7), the most important energy-absorption mechanism is shear plugging, which reaches 60% for a geometry ratio of 1.6. Since the friction is formulated in a spatial variable, it cannot be represented vs. time. Therefore, Fig. 7 shows only Stage 1 of the penetration process and the remaining energy of the projectile is absorbed by friction in Stage 2. Friction is the second energy-absorption mechanism in importance. The third energy-absorption mechanism in order of importance is compression in Region 1. These three energy-absorption mechanisms absorb almost 90% of the total projectile energy. Compression in Region 2, tensile failure of fibres, delamination and matrix cracking are the less important energy-absorption mechanisms.

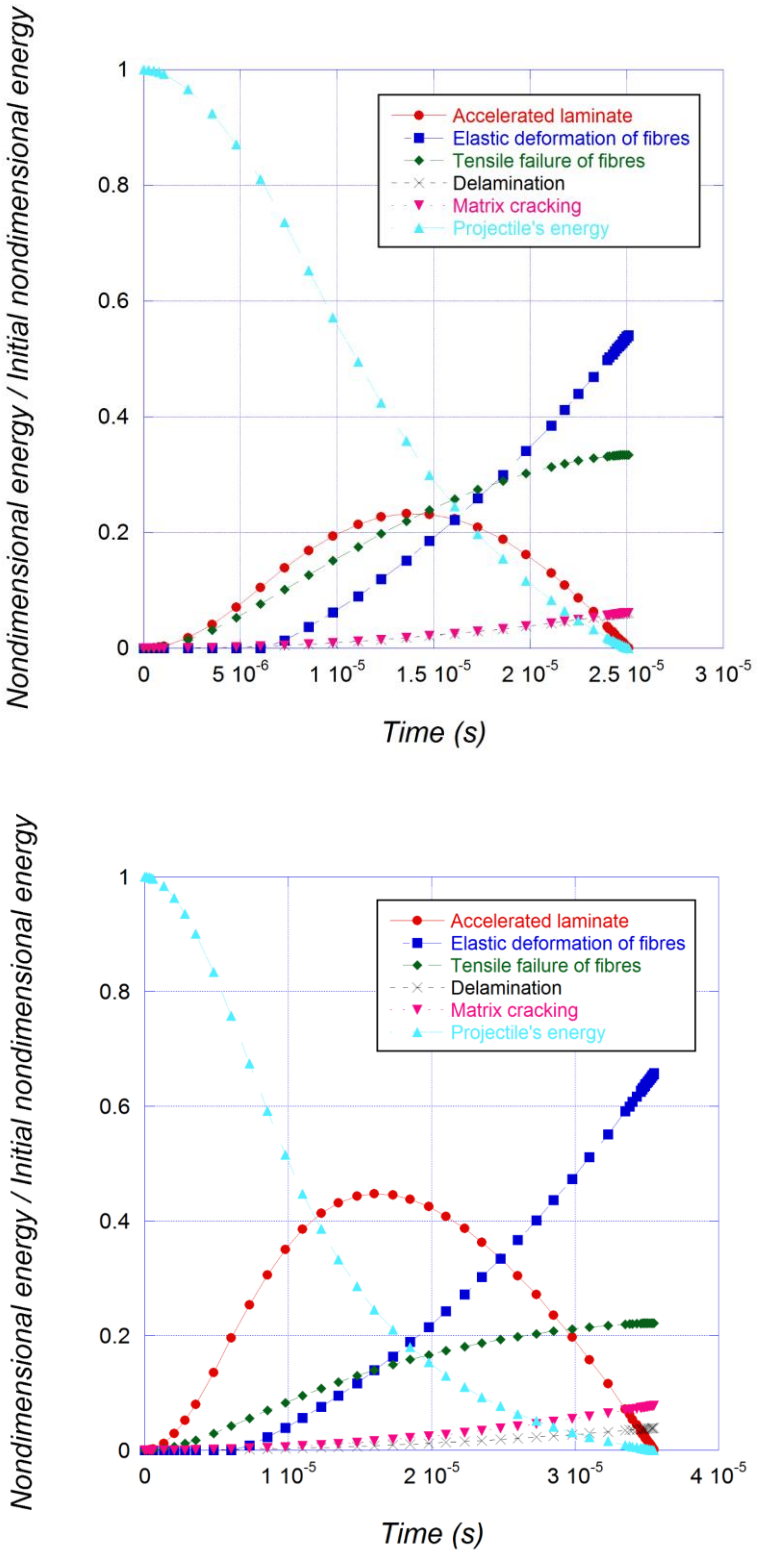


*Fig. 6. Nondimensional energy-absorption mechanisms for a woven laminate of E-Glass/polyester. (a) geometry ratio equal to 0.4, (b) geometry ratio equal to 0.8*

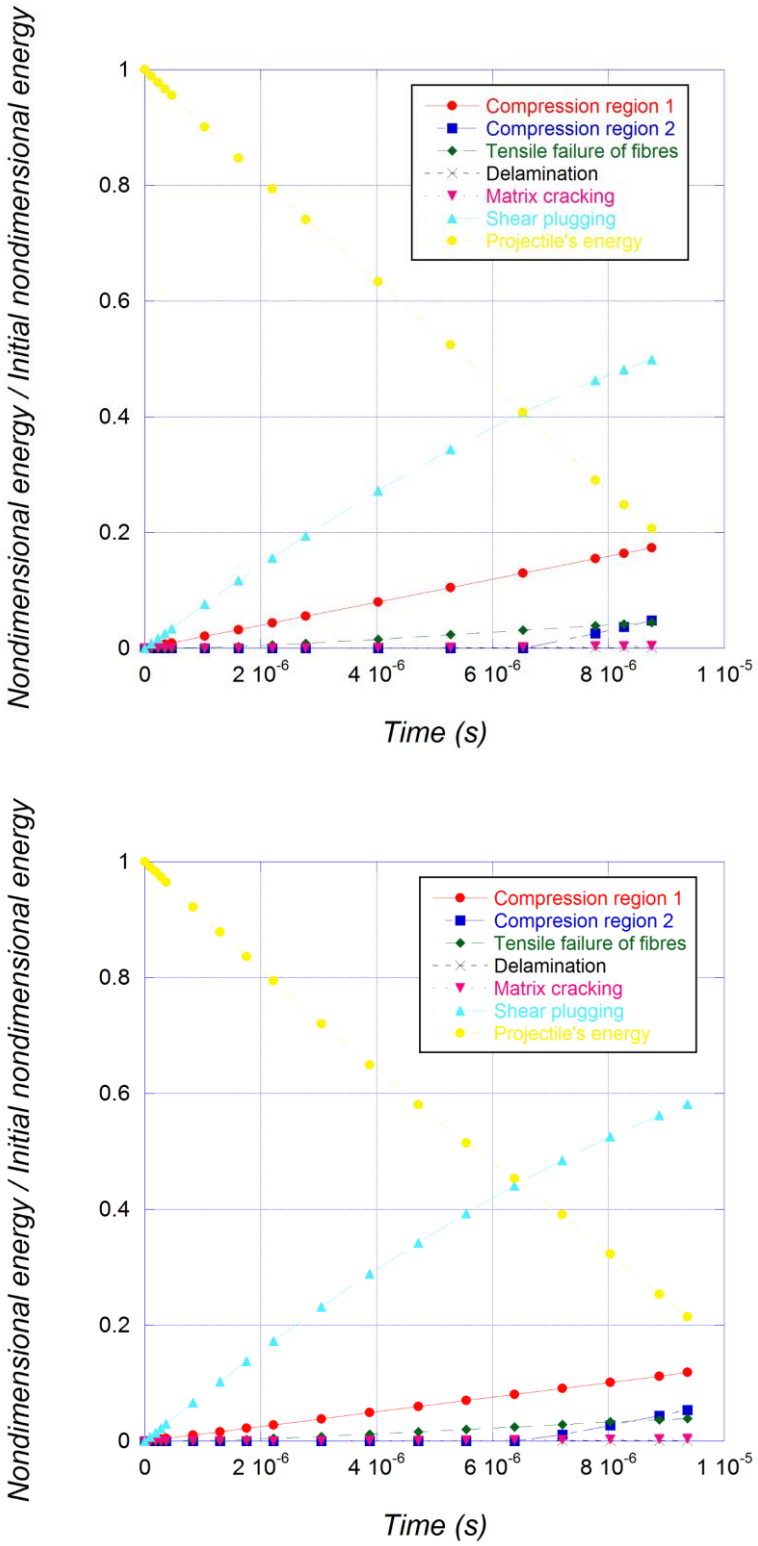


*Fig. 7. Nondimensional energy-absorption mechanisms for a woven laminate of E-Glass/polyester. (a) geometry ratio equal to 1.2, (b) geometry ratio equal to 1.6*

**6.- Conclusions**

In this paper a nondimensional formulation of two different analytical models has been developed, one for thin and another for thick woven E-Glass/polyester laminates, both impacted by a foreign object. The

application of the two models enabled the establishment of the threshold from which a laminate behaving as a thin one begins to perform as a thick composite. As in problems of impact on metal targets, when the geometry ratio (laminate thickness/projectile diameter) reaches a value near one, both models predict similar results and this finding clearly shows the transition from thin to thick laminate models.

The analytical model developed for thick laminates allowed the prediction of the ballistic limit with an error less than 1.5%. For the case of thin laminates, the maximum error of the predicted value of the ballistic limit of the model was approximately 10%.

The analytical model for thin laminates showed that the ballistic limit is independent of the geometry (spherical or cylindrical) of the projectile.

Both of the models (for thin and thick laminates) permit a check on how they participate in withstanding the projectile. The most important energy-absorption mechanisms are elastic deformation of fibres and tensile failure of fibres for thin laminates when the projectile velocity is near the ballistic limit. However, for the case of thick laminates the most important energy-absorption mechanisms when projectile velocity is close to the ballistic limit are shear plugging, friction and the compression that occurs just below the projectile (Region 1).

Also the energy absorbed by matrix cracking and delamination are not as important as the mechanisms defined above, regardless of the laminate thickness.

**Acknowledgements**

The authors are indebted to the project "Acción Estratégica en Materiales Compuestos y Análisis Numérico simplificado de Estructuras y protecciones ligeras sometidas a impacto balístico" (2010/00309/002) of the University Carlos III of Madrid for the financial support of this work.

**References**

1. Fatt MSH, Lin C. Perforation of clamped, woven E-glass/polyester panels. Compos Part B: Eng 2004 35(5), 359-378.
2. Walter TR, Subhash G, Sankar BV, Yen CF. Damage modes in 3D glass fiber epoxy woven composites under high rate of impact loading. Compos Part B: Eng 2009;40(6):584-589.
3. Reddy TS, Reddy PRS, Madhu V. Response of E-glass/Epoxy and Dyneema® composite laminates subjected to low and high velocity impact. Procedia Eng 2017;173, 278-285.
4. Buitrago BL, García-Castillo SK, Barbero E. Experimental analysis of perforation of glass/polyester structures subjected to high-velocity impact. Mat Lett 2010;64:1052-1054.

5. Rhymer J, Kim H, Roach D. The damage resistance of quasi-isotropic carbon/epoxy composite tape laminates impacted by high velocity ice. Compos Part A Appl S 2012;43(7): 1134-1144.
6. De Rosa IM, Dhakal HN, Santulli C, Sarasini F, Zhang ZY. Post-impact static and cyclic flexural characterisation of hemp fibre reinforced laminates. Compos Part B: Eng 2012;43(3):1382-1396.
7. Sanchez-Saez S, Barbero E, Zaera R, Navarro C. Compression after impact of thin composite laminates. Compos Sci Technol 2005;65(13):1911-1919.
8. Fujii K, Aoki M, Kiuchi N, Yasuda E, Tanabe Y. Impact perforation behaviour of CFRPs using high-velocity steel sphere. Int J Impact Eng 2002;27: 497-508.
9. Focht JR, Vinson JR. Predicting Ballistic Penetration and the Ballistic Limit in Composite Material Structures. AIAA J 2002;40(11):2366-2368.
10. Hazell PJ, Kister G, Stennett C, Bourque P, Cooper G. Normal and oblique penetration of woven CFRP laminates by a high velocity steel sphere. Compos Part A- Appl S 2008;39(5):866-874.
11. Yashiro S, Ogi K, Nakamura T, Yoshimura A. Characterization of high-velocity impact damage in CFRP laminates: Part I - Experiment. Compos Part A- Appl S 2013;48:93-100.
12. Garcia-Castillo SK, Navarro C, Barbero E. Damage in preloaded glass/vinylester composite panels subjected to high-velocity impacts. Mech Res Commun 2014;55: 66-71.
13. Bresciani, LM, Manes A, Ruggiero A, Iannitti G, Giglio M. Experimental tests and numerical modelling of ballistic impacts against Kevlar 29 plain-woven fabrics with an epoxy matrix: Macro-homogeneous and Meso-heterogeneous approaches. Compos Part B: Eng 2016; 88, 114-130.
14. Silva MAG, Cismaşiu C, Chiorean CG. Numerical simulation of ballistic impact on composite laminates. Int J Impact Eng 2005;31:289-306.
15. Ansari MM, Chakrabarti A, Iqbal, MA. An experimental and finite element investigation of the ballistic performance of laminated GFRP composite target. Compos Part B: Eng 2017; 125:211-226.
16. Gower HL, Cronin DS, Plumtree A. Ballistic impact response of laminated composite panels. Int J Impact Eng 2008;35:1000-1008.
17. García-Castillo SK, Sánchez-Sáez S, Santiuste C, Navarro C, Barbero E. Perforation of Composite Laminate Subjected to Dynamic Loads. In: Abrate S, Castanié B, Yapa DSY, editors. Dynamic Failure of Composite and Sandwich Structures. Netherlands: Springer, 2013. p. 291-337.
18. Chu TL, Ha-Minh C, Imad A. A numerical investigation of the influence of yarn mechanical and physical properties on the ballistic impact behavior of a Kevlar KM2® woven fabric. Compos Part B:

Eng 2016;95:144-154.

19. Vinson JR, Walter JM. Ballistic impact of thin-walled composite structures. AIAA J 1997;35:875-878.
20. Morye SS, Hine PJ, Duckett RA, Carr DJ, Ward IM. Modelling of the energy absorption by polymer composites upon ballistic impact. Compos Sci Technol 2000;60:2631-2640.
21. Wen HM. Predicting the penetration and perforation of FRP laminates struck normally by projectiles with different nose shapes. Compos Struct 2000;49(3):321-329.
22. Naik NK., Shrirao P. Composite structures under ballistic impact. Compos Struct 2004;66(1-4):579-590.
23. Mamivand M, Liaghat GH. A model for ballistic impact on multi-layer fabric targets. Int J Impact Eng 2010;37:806-812.
24. Nair NS, Kumar CVS, Naik NK. Ballistic impact performance of composite targets. Mater Des 2013;51:833-846.
25. Buitrago BL., García-Castillo SK., Barbero E. Influence of shear plugging in the energy absorbed by thin carbon-fibre laminates subjected to high-velocity impacts. Compos Part B: Eng 2013 49, 86-92.
26. Sikarwar RS, Velmurugan R, Gupta NK. Influence of fiber orientation and thickness on the response of glass/epoxy composites subjected to impact loading. Compos Part B: Eng 2014;60, 627-636.
27. Bresciani LM, Manes A, Giglio M. An analytical model for ballistic impacts against plain-woven fabrics with a polymeric matrix. Int J Impact Eng 2015;78:138-149.
28. MIL-STD-662F Standard. V50 Ballistic test for armor. Department of Defense Test Method Standard, 1997.
29. Zhu G, Goldsmith W, Dharan CKH. Penetration of laminated Kevlar by projectiles-II. Analytical model, Int J Solids Struct 1992; 29:421-436.
30. Potti SV, Sun CT. Prediction of impact induced penetration and delamination in thick composite laminates. Int J Impact Eng 1997;19(1):31-48.
31. Gellert EP., Cimpoeru SJ, Woodward R.L. A study of the effect of target thickness on the ballistic perforation of glass-fibre-reinforced plastic composites. Int J Impact Eng 2000;24(5):445-456.
32. Wen HM. Penetration and perforation of thick FRP laminates. Compos Sci Technol 2001; 61(8):1163-1172.
33. Naik NK, Shrirao P, Reddy BCK. (2005). Ballistic impact behaviour of woven fabric composites:

Parametric studies. Mater Sci Eng A-Struct Mater Prop Microstruct Process 2005;412(1):104-116.

34. Caprino G, Lopresto V, Santoro D. Ballistic impact behaviour of stitched graphite/epoxy laminates. Compos Sci Technol 2007;67(3):325-335.
35. Naik NK, Doshi, AV. Ballistic impact behaviour of thick composites: Parametric studies. Compos Struct 2008;82(3):447-464.
36. García-Castillo SK, Sánchez-Sáez S., Barbero E. (2012). Influence of areal density on the energy absorbed by thin composite plates subjected to high-velocity impacts. The Journal of Strain Analysis for Engineering Design, 47(7), 444-452.
37. Pandya KS, Shaktivesh S, Gowtham HL, Inani A, Naik NK. Shear Plugging and Frictional Behaviour of Composites and Fabrics Under Quasi-static Loading. Strain 2015;51(5):419-426.
38. ASTM Standard D 732-02.
39. García-Castillo SK, Sánchez-Sáez S, Barbero E. Nondimensional analysis of ballistic impact on thin woven laminate plates. Int J Impact Eng 2012;39(1):8-15.
40. Rosenberg Z, Dekel E. (2012). Plate perforation. In: Terminal ballistics. Berlin: Springer, 2012. p. 267-291.

Figure Caption



Table caption